Dislocation properties of coesite from an *ab-initio* parametrized interatomic potential

L. Giacomazzi,[1] P. Carrez,[2] S. Scandolo,[1] and P. Cordier[2]

[1]*CNR-IOM/Democritos National Simulation Center and the Abdus Salam International Centre for Theoretical Physics (ICTP), Strada Costiera 11, I-34151, Trieste, Italy*

[2]*Unité Matériaux et Transformations, Université Lille 1, Cité Scientifique, Bâtiment C6, 59655 Villeneuve d'Ascq, France*

(Received 13 April 2010; revised manuscript received 25 October 2010; published 31 January 2011)

Calculation of the properties of dislocations by computer simulations requires, among other things, the availability of accurate interatomic potentials, ideally with *ab-initio* quality. For crystals with large unit cells and complex crystal structures, such as most minerals, the number and size of the calculations may severely limit the applicability of a full *ab-initio* approach. In this paper we present an investigation of the dislocation properties of coesite, a mineral with a relatively large unit cell, carried out with a force field developed for silica based on a parametrization to *ab-initio* data. Two-dimensional generalized stacking fault energy surfaces for basal and prismatic planes are considered for a global search of the possible dissociation paths in partial dislocations. Test calculations show negligible differences between the energy surfaces calculated with the force field and with *ab-initio* methods. Five different coesite slip systems are investigated: [100](010), [001](010), [101](010), [010](001), and [010]($\bar{1}$01). Dislocation core structures and critical stresses are determined by using the Peierls-Nabarro-Galerkin approach. While [100] and [101] (screw) dislocations share a similar core structure, [001] differs substantially by showing a much larger split between partial dislocations. The lattice friction experienced by [001](010) is found to be close to those of [100](010) and [101](010), confirming the pseudohexagonal symmetry suggested by experiments.

DOI: 10.1103/PhysRevB.83.014110 PACS number(s): 61.72.Lk

I. INTRODUCTION

Understanding the plastic behavior of minerals is of paramount importance for unveiling the mechanisms behind the rheology of the solid Earth.[1] Modeling the rheology of minerals requires the description of plastic flow over different length scales, from the continuum limit down to the atomistic scale.

The structural complexity displayed by minerals, particularly those present in the crust and in the upper mantle, considerably increases the difficulty of an atomistic description of their plastic properties. Large unit cells, many atomic species, several inequivalent crystallographic planes, and multiple choices for the slip systems imply that a large number of atomistic level calculations need to be performed in order to obtain a complete picture of the energetics of the fundamental processes underlying plastic flow. In this context, computationally demanding approaches such as those based on *ab-initio* methods might have a limited range of applicability, and alternative approaches, yet retaining a similar quality of description of the interatomic interactions, might have to be sought.

In this paper we focus on the rheological properties of coesite as an example of a mineral with a simple chemical formula (SiO_2), but with a complex crystal structure. Coesite is the highest-density SiO_2 polymorph in which silicon is tetrahedrally coordinated to oxygen.[2] The coesite structure has a low crystal symmetry (monoclinic space group $C2/c$).[3] At ambient conditions the cell parameters are $a = 0.713\,56$, $b = 1.236\,92$, and $c = 0.717\,36$ nm, with $\beta = 120.34°$, and the unit cell contains 16 SiO_2 molecular units.[4] Coesite is the thermodynamically stable phase of SiO_2 above 2.5 GPa. In metamorphic rocks, coesite is one of the best mineral indicators of metamorphism at very high pressures [ultra-high-pressure (UHP) metamorphism[5,6]]. Such UHP metamorphic rocks record subduction or continental collisions in which crustal rocks have been carried to depths of about a 100 km before being brought to to the surface and exposed. Despite its geological relevance, the deformation processes, slip systems, and rheological laws of coesite are still unclear.[7–9]

The monoclinic coesite lattice has almost hexagonal parameters and it is possible to describe the coesite structure within a pseudohexagonal cell. This characteristic has implications for the nature of crystal defects as shown by the occurrence of (021) twinning which is related to this pseudosymmetry.[10] Following the same lines, Idrissi *et al.*[9] have shown that the diversity of dislocation Burgers vectors characterized by large-angle convergent-beam electron diffraction could be conveniently described in the pseudohexagonal setting. By contrast, as it appears from Fig. 1, the atomic arrangement in the primitive cell does not show either a threefold or a sixfold symmetry. Indeed, the view of the basal plane (010) of coesite (Fig. 1) shows a structure made of chains of four-membered rings of SiO_4 tetrahedra aligned parallel to the c direction. Furthermore, in the study of Idrissi *et al.*[9] the activation of pseudoequivalent $\frac{1}{3}\langle 11\bar{2}0\rangle$, i.e., [100], [001], and [101], dislocations appeared uneven, raising the question of possibly different mobilities as a consequence of different atomic core structures. Evidence of activation of [010] dislocations was reported, maybe as a consequence of a dissociation mechanism.[9] $\frac{1}{2}$[110] dislocations have also been observed, though much less frequently than $\frac{1}{3}\langle 11\bar{2}0\rangle$ dislocations.[9] All these experimental observations call for a detailed theoretical investigation of the main slip systems in coesite.

In this work we adopt a highly accurate interatomic potential [the Tangney and Scandolo (TS) force field[11]] to calculate generalized stacking fault energy surfaces (γ surfaces) of coesite. We show that calculations that would be considerably costly if done by *ab-initio* methods can instead be done with

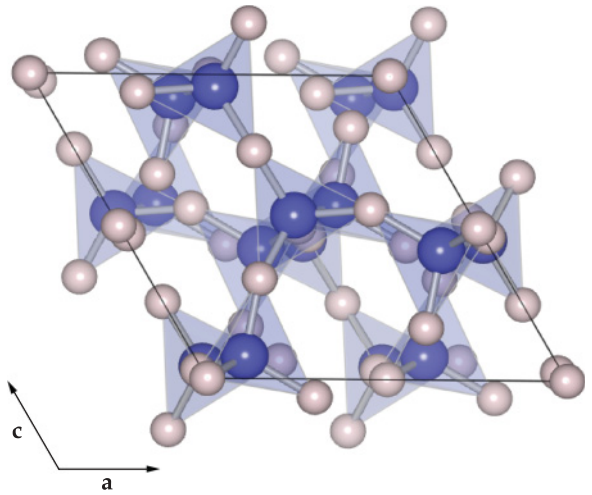

FIG. 1. (Color online) Ball and stick model of the coesite primitive cell: view of the (010) basal plane. Silicon and oxygen atoms are shown with blue (large) and light gray (small) balls.

a comparable quality by means of *ab-initio* parametrized potentials.[11–14] For modeling plastic deformation of materials on a large scale, ideally macroscopic, it becomes necessary to bridge from the atomistic description to a continuum one. This is done by informing a macroscopic model with atomistic data. In this work we apply the Peierls-Nabarro Galerkin (PNG) model[15,16] (Sec. II) to calculate dislocation properties in coesite such as core structures and behavior under applied stress. By discussing the activation of slip systems we aim at completing the available experimental information and hence at improving the current classification of dislocations in coesite.

The paper is organized as follows. The introduction of the work is presented in Sec. I. In Sec. II, we report the technical details of our calculations. First, in Sec. II A a brief outline of the PNG model is given. Next, in Sec. II B we discuss the adopted procedure for building supercells for calculating γ surfaces. We then address the structural properties of coesite and report the calculated elastic constants for the adopted TS force field (Sec. II C). Moreover, the TS force field is compared with that of van Beest, Kramer, and van Santen (BKS) force field and with *ab-initio* results for the calculation of a test γ line. In Sec. III A we present our results for the investigated slip systems: γ surfaces, dislocations, core structures, profiles (Sec. III B), and critical stresses (Sec. III C). Finally, Sec. IV contains the conclusions of our work.

II. METHODS AND TECHNICAL DETAILS

Over the years a model that has been largely adopted for finding dislocation properties such as dislocation size and Peierls stress is the Peierls-Nabarro (PN) model.[17–21] This model successfully combines a continuum description of the material with atomistic information concerning the dislocation core. The PN model originally expressed by an analytic formulation[17,18,22] became later very appealing when first-principles techniques successfully allowed the calculation of the generalized stacking fault energies[23] and hence of the dislocation properties for covalent materials such as silicon.[24] Several formulations of the PN model have been developed that can be applied also to nonplanar core dislocations.[19,21,25–28] The advent of first-principles approaches has led to the investigation of dislocation properties for a large variety of materials.[29–31] In the last decade this model has successfully helped in the understanding of the rheological behavior of mantle minerals such as olivine, ringwoodite, and $MgSiO_3$-perovskite.[30,32–35]

A. Peierls-Nabarro-Galerkin model

The complexity of the coesite structure in principle might allow dislocations with nonplanar cores. To investigate such a possible scenario, in this work we made use of the Peierls-Nabarro-Galerkin model. The PNG model is a generalization of the PN model recently formulated within the framework of finite-element techniques.[15,16] The PNG model allows several glide planes to be taken into account simultaneously and complex (possibly three-dimensional) cores to be calculated. As in the initial PN model, the dislocation core structure is obtained by the minimization of an elastic energy and of an interplanar potential. The latter is a function of the γ-surface energies from which the linear elastic part has been subtracted.[15,16] In the PNG method, two distinct fields are used: $\mathbf{u}(\mathbf{r})$, a three-dimensional displacement field of the volume V, and a two-dimensional $\mathbf{S}(\mathbf{r})$ field, which is expressed in the normal basis of the plane of a given γ surface. As a dislocation is introduced into the calculation, a solution is found by minimizing the energy with respect to $\mathbf{u}$ and $\mathbf{S}$, using a nodal mesh of at least 12 nodes per Burgers vector dimension to ensure the accuracy of the calculation.

A PNG simulation consists of three steps. First, we introduce a Volterra dislocation in a finite volume, the boundary of which is obtained by imposing the displacement of the result of the elastic solution of the corresponding dislocation.[36] The imposed boundary conditions are therefore consistent with a dislocation in an infinite medium, without any influence on the core structure. Next, the equilibrium of the displacement jump field $\mathbf{S}$ is determined at each node through a viscous relaxation scheme.[15,16] The last step of the calculation corresponds to the evaluation of the Peierls stress. As the relaxed core structure is reached, a strain is applied to the simulation cell. The level of strain is increased very slowly to mimic a quasistatic loading of the bulk of the material. Under such conditions, the Peierls stress can be determined when the relaxed dislocation core structure has moved from its initial position to the next equilibrium position.

B. γ surface

By the generalized stacking fault energy surface or γ surface, we mean the interplanar potential energy resulting from the rigid-body shear of a semi-infinite crystal over the other half crystal.[29] The calculation of the γ surface for a given slip system requires a supercell with a geometry that should be carefully designed for the shear plane and direction under investigation. Among several possibilities,[37,38] we have chosen to build supercells on a Cartesian reference frame defined by the normal of the stacking fault plane and by the shear direction. A vacuum buffer is added in the direction normal to

the slip plane to avoid interaction between repeated stacking faults resulting from the use of periodic boundary conditions. A set of shear displacement vectors spanning the chosen shear plane is introduced. The upper part of the supercell is then displaced for each displacement vector of the set and the excess energy is calculated, resulting in the γ surface of the chosen shear plane. All atoms except those located close to the vacuum region are allowed to relax in the directions perpendicular to the shear direction in order to minimize the energy of the γ surface. We built four distinct supercells for the γ-surface calculations of the (010), (100), (001), and $(10\bar{1})$ planes. In the pseudohexagonal setting, (010) corresponds to the basal plane {0001} containing the pseudoequivalent directions $\frac{1}{3}\langle\bar{1}2\bar{1}0\rangle$ that in the monoclinic notation are written as [100], [001], and [101]. The planes (001), (100) and $(\bar{1}01)$ correspond to the prismatic planes $\{\bar{1}100\}$. Supercells of 144 and 192 atoms were used for calculations on the basal plane and prismatic planes, respectively. Vacuum buffers of about 90 Å were used. In Fig. 2 we show the adopted supercell for the calculation of the basal plane γ surface. Note that the choice of the shear plane is not straightforward in general and some tests of the possible choices are required. In Fig. 2(ii) we show for example two planes among those we considered for the basal plane. Other parallel planes were considered, for instance those crossing more than one Si-O bond of a given tetrahedron.

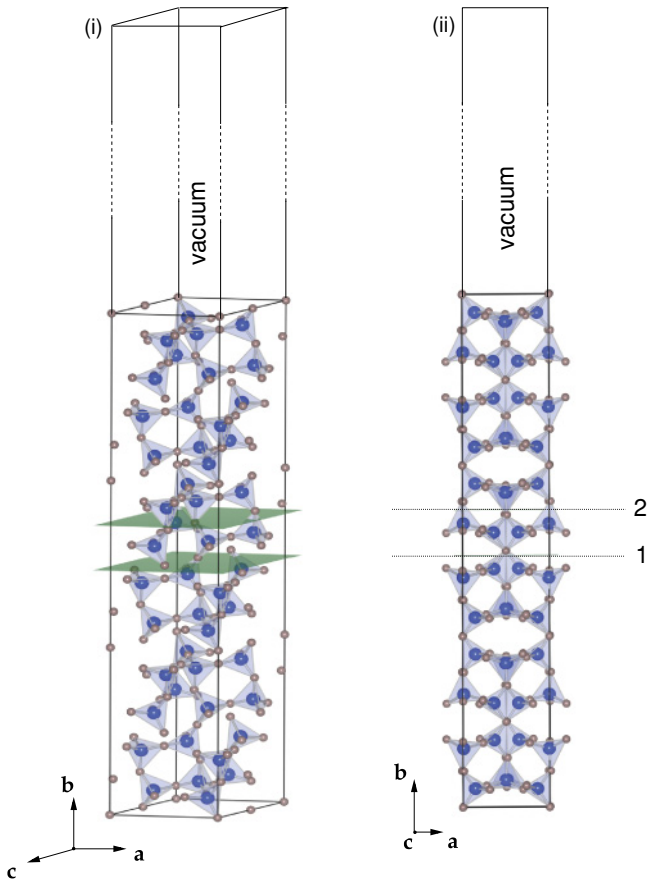

FIG. 2. (Color online) (i) Supercell used for the γ-surface calculation on the basal plane (010). (ii) Shear plane along which the γ surface of Fig. 4(a) was calculated (1) and a test choice for the shear plane (2) are shown.

We found that such choices are energetically unfavored with respect to those depicted in Fig. 2. In total we calculated more than ten different γ surfaces, each one defined by a grid of 20×20 points. This grid provides a good resolution for mapping all the relevant features of the γ surfaces.[39]

C. Force field

For calculating γ surfaces we take advantage of the TS force field for silica, the parameters of which were extracted from *ab-initio* calculations.[11] This force field actually matches both the requirements of being almost as accurate as *ab-initio* calculations and also less expensive. Furthermore, the TS force field successfully predicts the structures of liquid silica and the low-pressure crystalline silica structures.[11] We note that the TS force field is known to perform systematically better than other classical force fields for polymorphs in which the silicon atoms are fourfold coordinated.[12] For instance, the TS force field successfully predicts the c/a anomaly at the α-β transition in quartz, the density of states in α-quartz, the stability of cristobalite and tridymite, and the shape of the SiO_4 units in quartz at room temperature. Moreover, the TS force field successfully predicts phase transitions between quartz and coesite and between coesite and stishovite.[40] The calculated cell parameters of coesite at ambient conditions are in close agreement with the experimental values.[4,11] The a and c lattice parameters are almost identical: 7.162 Å and 7.165 Å, while b is 12.377 Å, and the angle β is 120.44°.

Knowledge of the elastic properties of the mineral is important in order to calculate dislocation properties properly. We calculated the elastic constants of coesite for the adopted force field at ambient pressure (0 GPa).[11] We derived them by applying strains (about 1%) to the primitive cell of coesite. These strains produce stresses which, by inverting Hooke's law, can be used to determine the elastic constants. The latter are an important input in the PNG model. In Table I we give the full elastic constant tensor together with the experimental values of Ref. 41. The calculation does not take temperature effects into account. We note that our calculated elastic constants show a departure from the experimental value that is comparable to or better than results obtained with other classical and *ab-initio* molecular dynamics approaches.[42,43]

The quality of the adopted interaction potential is further confirmed when γ surfaces are compared with those obtained by *ab-initio* calculations. As a test case we considered the projection of the basal plane γ surface along [001] ($\gamma_{[001]}$ line) for which we performed also first-principles calculations by using the QUANTUM-ESPRESSO code.[44,45] The result are shown

TABLE I. Ambient pressure (0 GPa) elastic constants of coesite as calculated in this work ($T = 0$ K) and as found from experiments (room temperature) in Ref. 41. Values are expressed in GPa.

	C_{11}	C_{12}	C_{13}	C_{15}	C_{22}	C_{23}	C_{25}
Expt.	160.8	82.1	102.9	−36.2	230.4	35.6	2.6
This work	163.0	66.31	80.6	−37.2	213.0	49.9	5.2
	C_{33}	C_{35}	C_{44}	C_{46}	C_{55}	C_{66}	
Expt.	231.6	−39.3	67.8	9.9	73.3	58.8	
This work	223.2	−31.8	46.8	10.4	65.6	56.8	

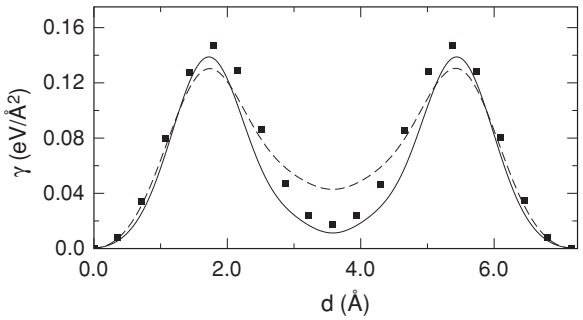

FIG. 3. γ line calculated by *ab-initio* method (dots), by *ab-initio* parametrized force field (solid), and by BKS force field (dashed) (Ref. 46). The adopted cell is shown in Fig. 2.

in Fig. 3 where we also compare with the results obtained with a very common classical force field for silica (BKS).[46] The BKS force field was used rather successfully for the study of structural, mechanical, and thermal properties of both crystalline and amorphous silica.[46,47] The γ line calculated with the adopted TS force field shows non-negligible deviations with respect to *ab-initio* data; still, the two maxima and the minimum between them are fairly well reproduced. In contrast, the BKS calculation gives a γ line where the two maxima are reasonably close to *ab-initio* data (about 13% difference), but the central minimum markedly differs from that of the *ab-initio* calculation. Interestingly enough, both the BKS and even more the TS force fields appear to be sufficiently accurate to describe the maxima of the γ surfaces even though the atomistic structure is locally very far from the equilibrium system.

Figure 3 also shows that γ-surface calculations constitute a quite strict benchmark for testing the quality of the chosen force field.

III. RESULTS

A. γ surfaces

The calculated γ surfaces of (010), (001), (100), and $(\bar{1}01)$ planes are shown in Fig. 4.[48,49] For each plane we considered and calculated the γ surfaces corresponding to a few possible choices of parallel shear planes. For example, in Fig. 5 we show the γ surfaces obtained for the two parallel shear planes shown in Fig. 2(ii). Both γ surfaces show the same pattern of deep minima along the [001] cell edge. By constrast, most of the maxima are changed in both shape and height. This might come from a different number of broken bonds during the shear of these two parallel planes. Although in principle one should take into account both γ surfaces for investigating the dislocation behavior, in practical calculations we are forced to consider just one γ surface among those obtained by the possible parallel choices of the shear plane. Of the two shown in Fig. 5 we kept the one giving the lowest average γ surface [labeled as (1) in Fig. 2(ii)]. Analogous criteria were used for the choices of the γ surfaces of the other planes we considered in this work.

The contour plot of the γ surface obtained by displacements on (010) is shown in Fig. 4(a). We remark the presence of deep minima oriented along [001], while along [100] and [101] deep minima are alternated with shallow minima. This is further clarified in Fig. 6 where we compare the projections of the (010) γ surface along directions [100], [001], and [101]. These γ lines display a two-peak camel shape, with [001] showing the sharpest and lowest peaks. This difference shows the intrinsic monoclinic structure of coesite (shown also in the γ-surface structure) and the limits of the pseudohexagonal conceptual frame. In Figs. 4(b), 4(c), and 4(d) we show the γ surfaces obtained for the (001), (100), and $(\bar{1}01)$ planes. The first two appear quite similar, showing deep minima arranged along [110] or [011], while the latter $(\bar{1}01)$ γ surface exhibits a complex pattern of minima.

TABLE II. Parameters obtained from the γ-surface calculations. τ_{max} is the ideal shear stress; γ_{max} is the maximum value of the excess energy barrier.

	τ_{max} (GPa)	γ_{max} (J/m^2)
[100](010)	15.1	3.1
[001](010)	13.0	2.2
[101](010)	15.9	3.3
[010](001)	22.9	5.1
[010]$(\bar{1}01)$	28.6	4.5

A careful inspection of the γ surfaces provides a first guideline for understanding which slip systems might be activated in coesite. In particular, in Table II we report the ideal shear stresses (maximal slope along the chosen shear direction, τ_{max}) and maximum value of the excess energy barrier (γ_{max}) calculated for five γ lines. The γ lines $\gamma_{[100](010)}$ and $\gamma_{[101](010)}$ show very similar values for both τ_{max} and γ_{max}. We note that $\gamma_{[001](010)}$ shows the lowest values for both the ideal shear stress and the excess energy barrier. Finally, the γ lines $\gamma_{[010](001)}$ and $\gamma_{[010](\bar{1}01)}$ show larger γ_{max} and τ_{max} values, ranging from about one and half to two times those found for the γ lines in the (010) plane.

B. Dislocation core structures: Results of the PNG model

In hexagonal structures $\frac{1}{3}\langle\bar{1}2\bar{1}0\rangle$ dislocations are usually found to glide in the basal plane which corresponds very often to the easiest slip system. The study of Ref. 7 suggests that this applies to coesite as well. Hence we decided to begin our investigations by considering dislocations gliding in the basal plane. This allows us to discuss the pseudohexagonal issue in coesite.[9] We have also considered the case of [010] dislocations gliding in two prismatic planes: (100) and $(\bar{1}01)$. Pyramidal planes are not considered and are left for future extensive investigations that are beyond the scope of this work. However, we note that by considering basal and prismatic planes, we are still able to discuss the largest part of the experimental observations of Ref. 9.

In Fig. 7 we show the results obtained from PNG calculations for the [001](010) screw dislocation. The dislocation core is described through the shear profile $S(x)$. The results of the PNG calculation are given on a discrete grid of points. We fitted the results by an expansion in a series of arctangent functions (we used a total of six arctangent functions) to obtain a smooth function $S(x)$.[50] Hence we derive a smooth curve for

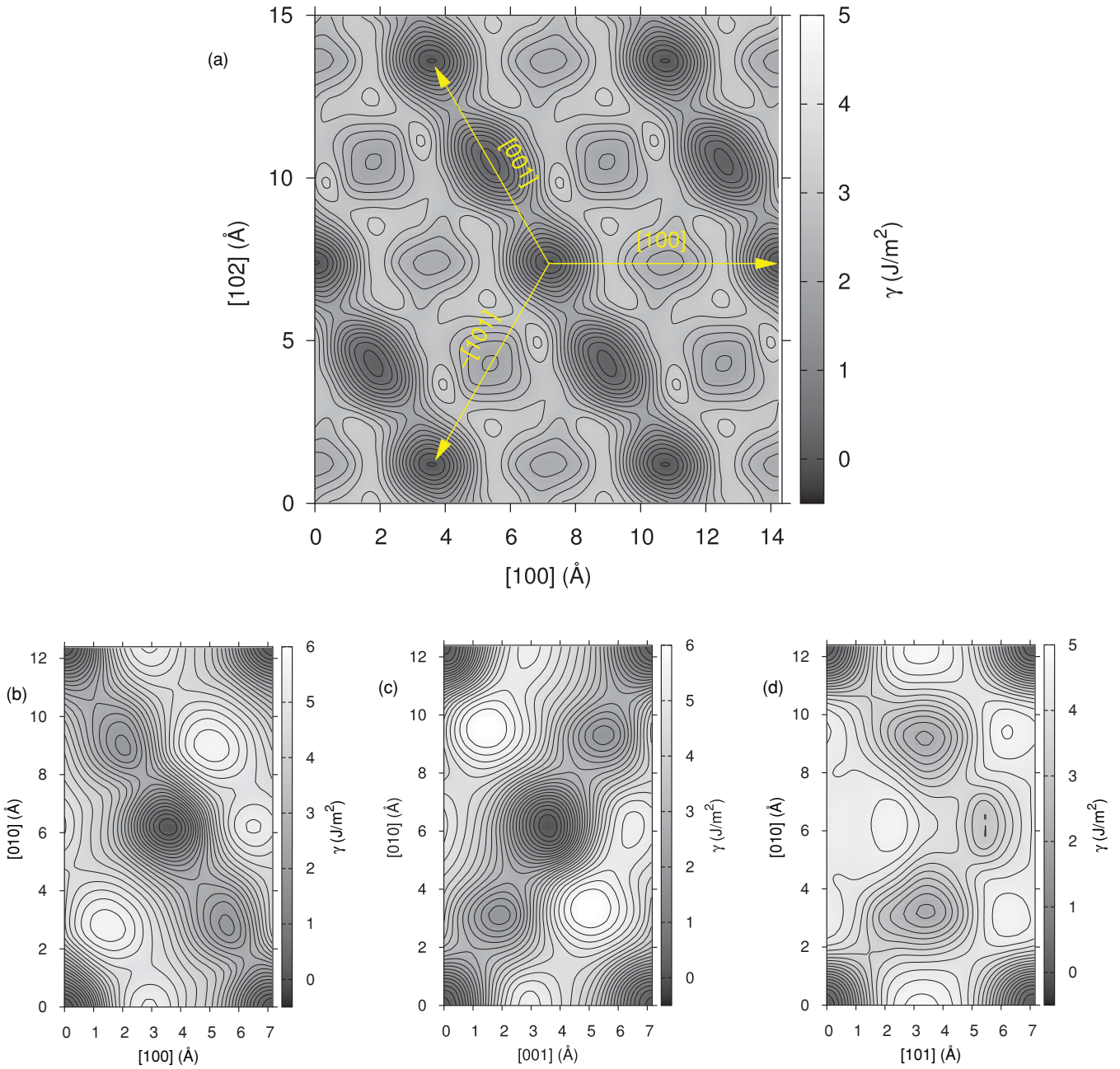

FIG. 4. (Color online) Contour plots of the γ surfaces of (a) (010), (b) (001), (c) (100), and (d) ($\bar{1}$01).

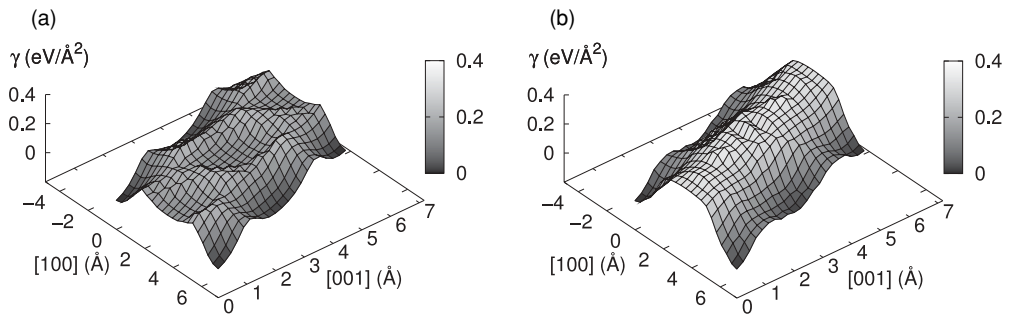

FIG. 5. γ surfaces obtained for the two parallel shear planes shown in Fig. 2(ii). (a) corresponds to the shear plane (1) and (b) to the shear plane (2). A mesh of 20 × 20 points was used.

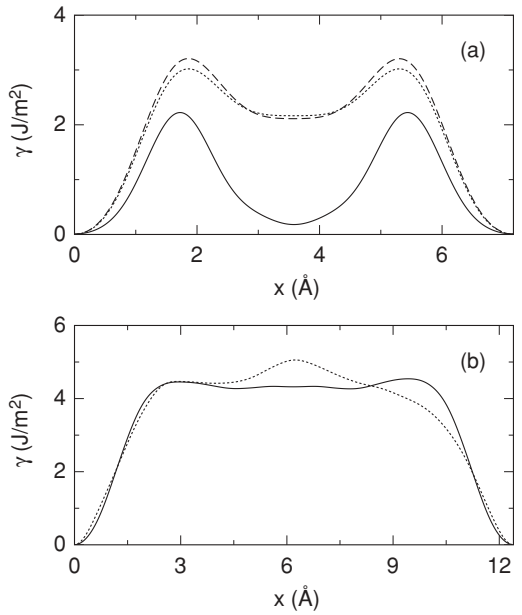

FIG. 6. (a) γ lines of the slip systems [100](010) (dotted), [001](010) (solid), and [101](010) (dashed). (b) γ lines of the slip systems [010](001) (dotted) and [010]($\bar{1}$01) (solid).

the dislocation density $\rho(x) = dS(x)/dx$ which is another way to look at the dislocation core. In Fig. 7, the two successive steps of the shear profile result in two well-separated peaks in the dislocation density profile, which are characteristic of two well-defined partial dislocations. The separation distance between the partials is ca. 20 Å. The energy of the stable stacking fault between the two partials is given by the minimum (at 50% shear) of the [001](010) γ line (Fig. 6), i.e., about 0.2 J/m^2.

In Figs. 8 and 9 we show the dislocation density profiles obtained with the PNG model for all the dislocations considered in this work. Correspondingly, in Table III we give the main parameters of the dislocation densities, i.e., the width at half maximum of the partial dislocation density, δ, which gives an estimate of the size of the dislocation core, and the separation Δ between partial dislocations.

In Fig. 8 we compare the local dislocation density profiles for the three [100](010), [001](010), and [101](010) screw dislocations. As for [001](010), [100](010) and [101](010)

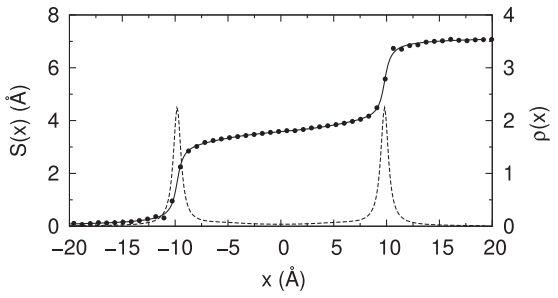

FIG. 7. Dislocation profiles $S(x)$ and $\rho(x) = dS(x)/dx$ (dotted) for the [001](010) screw dislocation. $S(x)$ calculated by PNG method (disks) is superimposed on the fit through an expansion in a series of arctangent functions (solid).

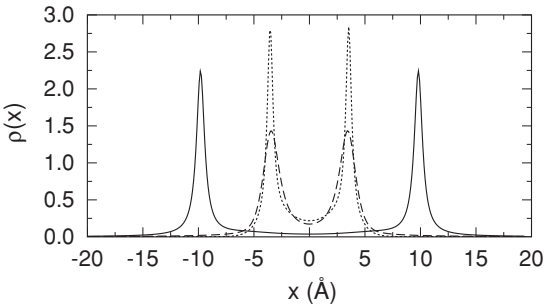

FIG. 8. Local dislocation densities for the screw [100](010) (dotted), [001](010) (solid), and [101](010) (dashed) dislocations.

screw dislocations exhibit dissociation into two well-defined partial dislocations. Their partial separation is identical (about 7 Å) and significantly smaller than that of [001](010). δ is very narrow and found to range between 0.5 and 1 Å.

Two [010] screw dislocations have been calculated. They were initially introduced in the (001) and in the ($\bar{1}$01) planes. In both cases, the dislocation spreads significantly but remains planar. In (001), the [010] screw dislocation is divided into four partial dislocations (Fig. 9). The separation of the outer partials is 11.2 Å. The [010] dislocation is also dissociated in the ($\bar{1}$01) plane. To a first approximation, the dislocation density profile (Fig. 9) can be described with only two partials. The separation Δ is 10.4 Å, close to the outer partial separation of [010](001). However, the two partials are relatively wide (δ about 1.7 Å) and their shapes suggest that each partial might be described by the superimposition of two narrower partials. Figure 10 shows that dissociation of [010] dislocations involves quite complex, noncollinear, dissociation paths. In ($\bar{1}$01), a small edge component appears because the dislocation paths getting close to a local minimum of the γ surface [Fig. 10(b)]. The tendency is the same in the (001) plane, but due to the symmetry in this plane, the dislocation exhibits two edge components of alternate signs [Fig. 10(a)].

In PNG calculations, the γ surfaces of the planes perpendicular to (or crossing) the initial glide plane are introduced automatically in order to reproduce the periodic variation of the crystal structure.[15,16] The dislocation could thus spread into these perpendicular planes. In spite of this freedom, however, all the investigated dislocations show planar cores.

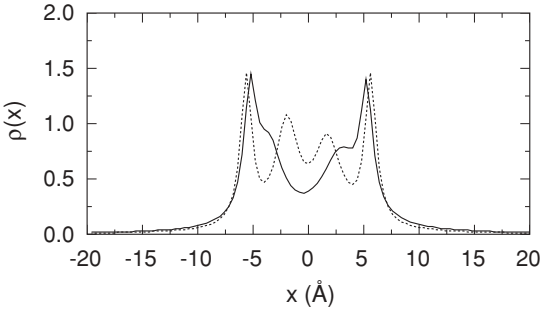

FIG. 9. Dislocation density profiles of the [010](001) (dotted) and [010]($\bar{1}$01) (solid) screw dislocations.

TABLE III. Results of the PNG model applied to the slip systems (screw) [100](010), [001](010), [101](010), [010](001), and [010]($\bar{1}$01). δ and Δ are the width at half maximum and the split between partial dislocations, respectively. σ_p is the critical shear stress (Peierls stress). The values given between parentheses give a statistical estimate of the uncertainty and are obtained by averaging calculations done by applying stresses in one direction and in the opposite one.

	δ (Å)	Δ (Å)	σ_p (GPa)
[100](010)	0.4	7	0.8 (0.2)
[001](010)	0.5	19.6	1 (0.2)
[101](010)	0.9	6.9	0.7 (0.2)
[010](001)	0.8	11.2	1.9
[010]($\bar{1}$01)	1.7	10.4	1.7

C. Peierls stresses

The Peierls stress σ_p is the minimum stress required to move a dislocation through a perfect crystal lattice without thermal activation. The PNG method allows for calculations of dislocation core structures under the presence of an applied stress.[15,35] The procedure used to calculate σ_p, as decribed in Ref. 16, corresponds to a slow straining of the simulation cell in order to detect at which strain level, and thus at which stress, the dislocation core moves from one Peierls valley to another. In Table III we summarize the results for Peierls stresses and dislocation splittings. Despite having different core structures, the three dislocations gliding in the (010) plane exhibit very comparable Peierls stresses with [001](010) only being slightly harder than the two others. The critical shear stresses found for [010] dislocations are significantly larger, by about a factor 2, with respect to those of dislocations gliding on the (010) plane. However, [010] slip could be activated because [010] dislocations can relax their cores by complex dissociations involving several partial dislocations (Figs. 9 and 10).

In addition to [100], [001], [101], and [010], dislocations showing Burgers vector $\frac{1}{2}$[110] have also been reported experimentally, though in a lower proportion with respect to the [100], [001], and [101] dislocations. Thus it is unlikely that $\frac{1}{2}$[110] dislocations have a lower σ_p than those found for [100], [001], and [101] dislocations. We note that the theoretical modeling of $\frac{1}{2}$[110] involves the treatment of pyramidal planes, which also, because of the previous remarks, appears as a complication beyond the scope of this work.

D. Discussion

Geometrical aspects have some implications for crystal defects. The proximity of the coesite structure with hexagonal symmetry is responsible, for instance, for (021) twinning,[10] and Idrissi *et al.*[9] have shown that description of dislocations within a pseudohexagonal framework could be instructive. However, Langenhorst and Poirier[8] had already pointed out earlier that hexagonal pseudosymmetry cannot be considered at the atomic scale. Indeed, Idrissi *et al.*[9] had observed some differences in the occurrence of [100], [001], and [101] dislocations and raised the question of differences in mobility and activation of these slip systems. The present study allows a quantitative answer to this question. Figure 4(a) shows that, according to the symmetry of the $C2/c$ space group, the highest symmetry in the (010) plane is a twofold axis. However, γ lines along the [100], [001], and [101] directions (Fig. 6) provide more quantitative information. If [100] and [101] are clearly not equivalent from the symmetry point of view, the resistance to shear along these directions is very similar and very few differences are expected between the related dislocations, as shown by the PNG modeling of their properties. On the other hand, [001] glide seems easier than [100] and [101] glide, as can be inferred from Fig. 6 and from the values of the ideal shear stresses (Table II). By contrast, the lattice friction experienced by this system is found to be very close to those of the other two. This study suggests that [100], [101], and [001] dislocations experience very similar lattice friction and hence should have similar mobilities. The differences of occurrence reported by Idrissi *et al.*[9] would thus be an observation bias, rather than reflecting intrinsic differences in the activation of these dislocations.

In their study, Idrissi *et al.*[9] reported also activation of [010] dislocations with some evidences of dissociation. Such spread core structures could be expected since [010] dislocations have

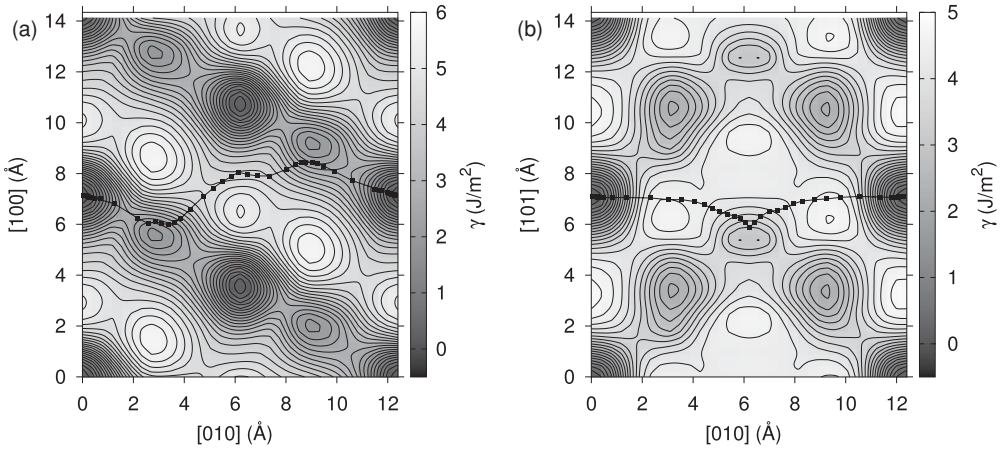

FIG. 10. γ surfaces (a) (001) and (b) ($\bar{1}$01) on which shear paths (line with filled squares) of the [010] screw dislocations have been superimposed.

a larger Burgers vector modulus than [100], [101], or [001] dislocations (12.4 Å, to be compared to ca. 7.1 Å). Figure 10 shows that dissociation is the result of the search for an easy shear path in the γ surfaces. In $(\bar{1}01)$ or (001), this gives rise to complicated, zigzag, shear paths which induce a dissociation into four partial dislocations. This suggests that the possibility for [010] dislocations to dissociate allows the activation of the [010] slip together with the [100], [101], and [001] slips as observed by Idrissi *et al.*[9]

IV. CONCLUSIONS

Modeling dislocations is still a quite challenging task, first because experimental data available for comparisons are usually rare and experimental information is often limited to just Burgers vectors. Furthermore, from a theoretical point of view, a fully atomistic simulation of dislocations is challenging due to the macroscopic extension of the defects. Thus it is necessary to rely on approximated models that combine atomistic information with a quasicontinuum or continuum description.

With the TS force field, we calculated the elastic constants of coesite, which are found to be reasonably close to the experimental ones. We show that γ surfaces calculated by the TS force field are comparable in quality with *ab-initio* results and much better than those obtained by more standard classical force fields such as the BKS. The TS force field allows us to calculate the γ surfaces of many different slip planes after checking several alternative planes for a given orientation. This is done with a low computational cost with respect to *ab-initio* methods, where the calculations depend severely on the size of the system as well as on the cell size.

The present study is a theoretical attempt to study dislocation properties in coesite. We exploit the capabilities of the TS force field and of the PNG model that we used to calculate dislocation core structures and Peierls stresses. We achieve an overall good description of the main slip systems for which we discuss about activation, dislocation size and splittings, and dissociation into noncollinear partials. We show that in order to understand dislocation properties such as dissociation in partial dislocations and gliding paths it is important to calculate the γ surfaces for each relevant slip plane, because information coming from single γ lines is limited. This work shows that the lattice friction experienced by the [001](010) slip system is close to those of [100](010) and [101](010) slip systems. This supports the pseudohexagonal symmetry description of dislocations in coesite that was suggested by recent experiments.

ACKNOWLEDGMENTS

We acknowledge support from Consiglio Nazionale delle Ricerche (CNR) and Centre National de la Recherche Scientifique (CNRS) through the project "EuroSlab" of the EuroMinScI/ESF initiative. L.G. acknowledges useful discussions with C. R. Miranda. P.C. acknowledges C. Denoual for his help in performing PNG calculations.

[1] S. Karato, *Deformation of Earth Materials: An Introduction to the Rheology of Solid Earth* (Cambridge University Press, New York, 2008).
[2] L. Coes, Science **118**, 131 (1953).
[3] R. J. Angel, C. S. J. Shaw, and G. V. Gibbs, Phys. Chem. Miner. **30**, 167 (2003).
[4] L. Levien and C. T. Prewitt, Am. Mineral. **66**, 324 (1981).
[5] C. Chopin, Contrib. Mineral. Petrol. **86**, 107 (1984).
[6] Z. Y. Zhao, C. J. Wei, and A. M. Fang, Earth Planet. Sci. Lett. **237**, 209 (2005).
[7] J. Renner, B. Stöckhert, A. Zerbian, K. Röller, and F. Rummel, J. Geophys. Res. **106**, 19411 (2001).
[8] F. Langenhorst and J. P. Poirier, Earth Planet. Sci. Lett. **203**, 793 (2002).
[9] H. Idrissi, P. Cordier, D. Jacob, and N. Walte, Eur. J. Mineral. **20**, 665 (2008).
[10] D. Jacob, P. Cordier, J. P. Morniroli, and H. P Schertl, Eur. J. Mineral. **20**, 119 (2008).
[11] P. Tangney and S. Scandolo, J. Chem. Phys. **117**, 8898 (2002).
[12] D. Herzbach, K. Binder, and M. H. Muser, J. Chem. Phys. **123**, 124711 (2005).
[13] D. Marrocchelli, M. Salanne, and P. A. Madden, J. Phys. Condens. Matter **22**, 152102 (2010).
[14] N. Ohtori, M. Salanne, and P. A. Madden, J. Chem. Phys. **130**, 104507 (2009).
[15] C. Denoual, Phys. Rev. B **70**, 024106 (2004).
[16] C. Denoual, Comput. Methods Appl. Mech. Eng. **196**, 1915 (2007).
[17] R. Peierls, Proc. Phys. Soc. London **52**, 34 (1940).
[18] F. R. N. Nabarro, Proc. Phys. Soc. London **59**, 256 (1947).
[19] G. Schoeck, Mater. Sci. Eng. A **400-401**, 7 (2005).
[20] G. Schoeck, Acta Mater. **54**, 4865 (2006).
[21] G. Lu, in *Handbook of Materials Modeling*, edited by S. Yip (Springer, Amsterdam, 2005), pp. 793–811.
[22] B. Joós, Q. Ren, and M. S. Duesbery, Phys. Rev. B **50**, 5890 (1994).
[23] E. Kaxiras and M. S. Duesbery, Phys. Rev. Lett. **70**, 3752 (1993); V. Vitek, Phys. Status Solidi **18**, 687 (1966); Philos. Mag. **18**, 773 (1968).
[24] Q. Ren, B. Joos, and M. S. Duesbery, Phys. Rev. B **52**, 13223 (1995).
[25] V. V. Bulatov and E. Kaxiras, Phys. Rev. Lett. **78**, 4221 (1997).
[26] L. Lejcek and F. Kroupa, Czech. J. Phys. B **26**, 528 (1976); **22**, 813 (1972).
[27] G. Lu, V. V. Bulatov, and N. Kioussis, Philos. Mag. **83**, 3539 (2003).
[28] A. H. W. Ngan, J. Mech. Phys. Solids **45**, 903 (1997); G. Schoeck, Philos. Mag. Lett. **77**, 141 (1998).
[29] Y.-M. Juan and E. Kaxiras, Philos. Mag. A **74**, 1367 (1996).
[30] D. Ferré, P. Carrez, and P. Cordier, Phys. Rev. B **77**, 014106 (2008).
[31] C. R. Miranda and S. Scandolo, Comput. Phys. Commun. **169**, 24 (2005).
[32] P. Carrez, D. Ferré, and P. Cordier, Nature (London) **446**, 68 (2007).
[33] P. Carrez, P. Cordier, D. Mainprice, and A. Tommasi, Eur. J. Mineral. **18**, 149 (2006).
[34] J. Durinck, P. Carrez, and P. Cordier, Eur. J. Mineral. **19**, 631 (2007).
[35] A. Metsue, P. Carrez, C. Denoual, D. Mainprice, and P. Cordier, Acta Mater. **58**, 1467 (2010).
[36] L. Pillon and C. Denoual, Philos. Mag. **89**, 127 (2009).

[37] V. V. Bulatov, W. Cai, R. Baran, and K. Kang, Philos. Mag. **86**, 2847 (2006).

[38] J.-An Yan, C.-Yu Wang, and S.-Ying Wang, Phys. Rev. B **70**, 174105 (2004).

[39] We note that, if the situation requires it, the adopted interaction potential (Sec. II) would allow for calculations with a finer grid or larger cells (more void) without becoming too costly, n contrast to *ab-initio* calculations.

[40] Y. Liang, C. R. Miranda, and S. Scandolo, Phys. Rev. Lett. **99**, 215504 (2007).

[41] D. J. Weidner and H. R. Carleton, J. Geophys. Res. **82**, 1334 (1977).

[42] K. de Boer, A. P. J. Jansen, R. A. van Santen, and S. C. Parker, Phys. Rev. B **53**, 14073 (1996); E. Bourova, S. C. Parker, and P. Richet, Phys. Chem. Miner. **31**, 569 (2004).

[43] H. Kimizuka, S. Ogata, and J. Li, J. Appl. Phys. **103**, 053506 (2008).

[44] [www.quantum-espresso.org].

[45] The exchange and correlation energy was accounted for through the local density approximation to density functional theory. Plane wave basis sets with energy cutoffs of 25 and 200 Ry were used to expand the electron wave functions and the electron density, respectively. Core-valence interactions were accounted for by a norm-conserving pseudopotential for Si (Ref. 51) and an ultrasoft one for O (Ref. 52).

[46] B. W. H. van Beest, G. J. Kramer, and R. A. van Santen, Phys. Rev. Lett. **64**, 1955 (1990).

[47] K. Vollmayr, W. Kob, and K. Binder, Phys. Rev. B **54**, 15808 (1996); S. N. Taraskin and S. R. Elliott, *ibid.* **56**, 8605 (1997).

[48] The γ surfaces shown in Fig. 4 are the result of an interpolation done on a fine grid. We checked that all the interpolated γ surfaces well reproduce the original ones. Small discrepancies were registered only around the maxima, therefore without affecting the PNG results.

[49] We calculated the γ surface of the basal plane for the coesite structure relaxed at 5 GPa. We did find only small increases (at most of about 10%) about the maxima, without any relevant change of shape. This suggests that the results obtained for dislocations in coesite at ambient conditions most likely can be considered meaningful up to several GPa.

[50] V. V. Bulatov and W. Cai, *Computer Simulations of Dislocations* (Oxford University Press, New York, 2006).

[51] G. B. Bachelet, D. R. Hamann, and M. Schlüter, Phys. Rev. B **26**, 4199 (1982).

[52] D. Vanderbilt, Phys. Rev. B **41**, 7892 (1990).